Applied Physics Letters ARTICLE pubs.aip.org/aip/apl

Deformation and motion of skyrmion bags driven by surface acoustic wave

Cite as: Appl. Phys. Lett. **126**, 252403 (2025); doi: 10.1063/5.0263722
Submitted: 6 February 2025 · Accepted: 8 June 2025 ·
Published Online: 24 June 2025

Shengbin Shi,[1] Yunhong Zhao,[2] Peng Han,[1] Jiajun Sun,[1] Rui Zhu,[1] and Jie Wang[1,2,a)]

AFFILIATIONS

[1]Department of Engineering Mechanics, Zhejiang University, Zheda Road 38, Hangzhou, Zhejiang 310027, Zhejiang, China
[2]Zhejiang Laboratory, Hangzhou, Zhejiang 311100, China

[a)]Author to whom correspondence should be addressed: jw@zju.edu.cn

ABSTRACT

Skyrmion bags are stable spin textured topologies with arbitrary topological charges, and have the potential to become new carriers in racetrack memory. After the discovery of skyrmion bags, the injection and driving methods of a single skyrmion are gradually applied to the manipulation of skyrmion bags. However, traditional methods, including spin current, magnetic anisotropic gradient, and spin waves generated by microwave fields, inevitably bring problems of high energy consumption and difficulty in miniaturization. With the development of strain electronics, acoustic waves have been widely used to manipulate magnetic topologies. Here, we numerically investigate the dynamical characteristic of skyrmion bags driven by surface acoustic waves. The results show that material damping and acoustic wave amplitude and frequency have a great influence on the skyrmion bag. With decrease in damping, the skyrmion bags move gradually faster. Also, increase in amplitude or frequency can generate similar effect on the velocity of skyrmion bags. Unlike acoustic wave-driven single skyrmions, the strong magnetoelastic coupling effect in the ferromagnetic film and the rich spin texture of skyrmion bags induce deformation in the skyrmion, along with a 38% increase in its velocity. Further, the deformation of the skyrmion is a combined effect of *in situ* rotation and breath caused by surface acoustic waves. This work demonstrates that the surface acoustic wave can be used to drive skyrmion bags, which offers potential applications for diverse storage of information based on the skyrmion bags in the future.

Individual magnetic skyrmions are stable particle-like spin configurations during the magnetization of chiral magnet[1–4] or Dzyaloshinskii–Moriya interaction (DMI) in ultrathin magnetic multilayers.[5–8] Due to its stable topological properties, small size, and ease of driving, it is widely used in building racetrack memory models.[9–11] However, in the current model, a single skyrmion only represents one logic bit of binary. The relatively long distance and the lateral deflection may lead to data loss as a result of interaction force and spin Hall effect of skyrmions, which limits the density and accuracy of information storage.[12,13] Therefore, there is an interest in higher topology skyrmions, which can encode more data per texture and increase the density of storage, while retaining the advantages of traditional skyrmions, i.e., good topological protection when passing through defects.[14] Many non-trivial noncollinear spin textures as variations and extensions of the skyrmion have also been predicted and observed.[15] In 2019, the skyrmion bag was experimentally discovered in liquid crystals[16] and then proposed in magnetic systems.[17–19] Subsequently, Tang *et al.* discovered magnetic skyrmion bags numerically and experimentally in thick FeGe plates using Lorentz transmission electron microscopy.[20] Skyrmion bags, as spin textures with arbitrary topological charge, are expected to become information carriers for multiple-data and high-density racetrack memory[14,20,21] and interconnect device.[22,23]

Skyrmion bags, called sacks, are nested skyrmionic structures of any integer topological degree, which are typically composed of a single skyrmion as an outer boundary and many inner skyrmions with opposite magnetization distribution compared with the former. In two-dimensional (2D) models describing thin films, skyrmion bags can be described by the total topological charge number defined as

$$Q = \frac{1}{4\pi}\int \boldsymbol{m}\cdot\left(\partial_x \boldsymbol{m}\times\partial_y \boldsymbol{m}\right)dxdy, \tag{1}$$

where $\boldsymbol{m}$ is the unit vector field of magnetization. Accordingly, the topological charge number of a single skyrmion is expressed as $Q = 1$ and that of the skyrmionium is $Q = 0$. Define S(N) as skyrmion bags with N inner skyrmions and the total topological charge number of $Q = 1 - N$. Different skyrmion bags are represented from S(2) to S(9) in Fig. 1(b).

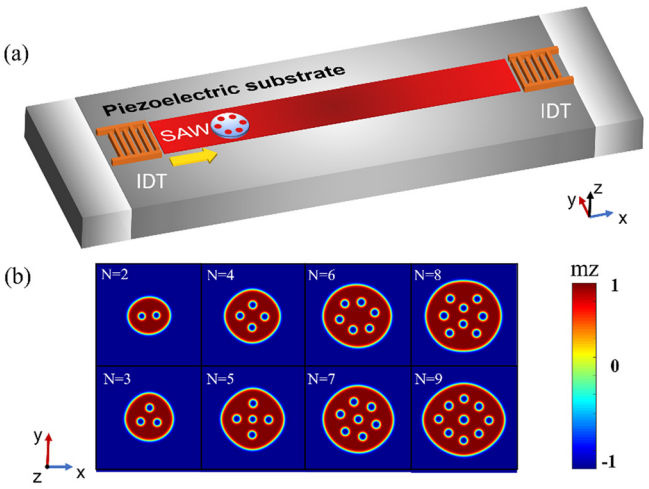

FIG. 1. (a) The schematic diagram of surface acoustic wave-driven skyrmion bags. The left orange IDT region represents the acoustic excitation source. The gray gradient area on both sides of the PZT substrate indicates the absorption boundary. (b) Stable magnetization distribution of skyrmion bags with N = 2–9.

For skyrmion bags-based device, it is very important to efficiently drive skyrmions bags with low-energy consumption. Intensive efforts have been devoted to driving skyrmion bags to achieve racetrack storage without altering the spin texture. Many approaches have been used to drive skyrmion bags, such as spin–orbit torques,[14] spin-transfer torques,[21] magnetic anisotropy gradient,[24] voltage gates,[22,25] and spin wave.[26] Nevertheless, the manipulation of skyrmion bags with low dissipation and low frequency still remains a problem. Therefore, it is necessary to explore a potentially efficient approach to drive skyrmion bags. Due to the magnetoelastic coupling effect of ferromagnetic materials, mechanical control of magnetic order through strain[27,28] and acoustic wave[29] has become a promising approach. In particular, surface acoustic waves (SAWs) are long-range carriers (wave propagating over millimeter distances through ferromagnets) for dynamic strain,[30–33] which have been used as an efficient method to generate[34,35] and move skyrmions[36,37] by SAW-induced spatiotemporally varying strain and inhomogeneous effective torques. Even if the topological charge number Q = 0, surface acoustic waves can be used to drive the skyrmionium.[38] Khoshlahni *et al.*[39] achieved the dynamics of a magnetic skyrmion induced by linear and circular surface acoustic waves in antiferromagnetic (AFM) systems. Due to the complex topology, it still remains a problem to acquire the dynamics of skyrmion bag driven by SAWs.

In this work, we numerically investigate the effect of surface acoustic waves on the driving of magnetic skyrmion bags. The dynamic evolution of the magnetization and displacement were obtained by combining the solution of the Landau–Lifshitz–Gilbert equation and the elastodynamics equation. We found that skyrmion bags can be effectively driven by acoustic waves, and their velocity can be adjusted by the regulation of material damping constant, frequency or amplitude of SAWs. Unlike the motion of a single skyrmion, the increased number of skyrmions in a bag introduces complex internal interactions, leading to significant deformation and a 38% increase in velocity during motion. Moreover, by scaling the simulation step, it can be observed that the mutation of skyrmion shape is derived from *in situ* rotation and breath of the skyrmion in the bag under periodic SAWs. The *in situ* rotation period coincides with the elastic wave period, while the breathing period coincides with the half-wavelength period. As distinguished from skyrmion intrinsic breathing and cyclotron modes,[40,41] the dynamic phenomenon of skyrmion bag is expected to provide a deeper understanding of complex spin texture. Our results reveal that the skyrmion bags can be driven by surface acoustic wave conveniently and efficiently, making them promising for application in racetrack memories.

For micromagnetic simulation, the magnetization dynamic of ferromagnetic materials is described by the LLG equation as follows:

$$\frac{\partial \boldsymbol{m}}{\partial t} = -\gamma \boldsymbol{m} \times \boldsymbol{H}_{eff} + \alpha\left(\boldsymbol{m} \times \frac{\partial \boldsymbol{m}}{\partial t}\right), \tag{2}$$

where $\boldsymbol{m}$ is the normalized magnetization vector, γ is the gyromagnetic ratio, α is the Gilbert damping constant, $H_{eff} = \frac{-1}{\mu_0 M_s}\frac{\delta E}{\delta \boldsymbol{m}}$ is the effective magnetic field, M_s is the saturation magnetization, μ_0 is the vacuum permeability. Here, E is the total energy comprised of the exchange energy, Dzyaloshinskii–Moriya interaction (DMI), magnetostatic energy, uniaxial anisotropy energy, elastic energy and magnetoelastic energy, which can be written as

$$\begin{aligned} E = {} & A(\nabla m_i)^2 + D(m_z \nabla \cdot m_i - m_i \nabla m_z) - \mu_0 \mathrm{m}_i M_s H_i \\ & - \frac{1}{2}\mu_0 m_i M_s H_{mag,i} - K_1\left(m_z^2\right) + \frac{1}{2} c_{ijkl}\varepsilon_{ij}\varepsilon_{kl} \\ & + B_1\left(\varepsilon_{xx}m_x^2 + \varepsilon_{yy}m_y^2 + \varepsilon_{zz}m_z^2\right) + B_2(\varepsilon_{xy}m_x m_y \\ & + \varepsilon_{yz}m_z m_y + \varepsilon_{xz}m_x m_z). \end{aligned} \tag{3}$$

Micromagnetic simulations based on the MuMax3 program[42] were performed to investigate the dynamic properties. Because of the introduction of the elastodynamic equation, an extension of MuMax3[43] was adopted to solve the real-time coupling of elasto-magneto-dynamical problems. In our simulation, an ultrathin wide ferromagnetic film with a size of $512 \times 512 \times 1\,\mathrm{nm}^3$ and a narrow strip of size $512 \times 120 \times 1\,\mathrm{nm}^3$ are considered with a cell size of $2 \times 2 \times 0.5\,\mathrm{nm}^3$, as shown in Fig. 1(a). The key input parameters are derived from Co/Pt films in experiments[44,45] and previous theoretical work:[21,36] $M_s = 5.8 \times 10^5\,\mathrm{A/m}$, $A = 1.0 \times 10^{-11}\,\mathrm{J/m}$, $D = 3.0 \times 10^{-3}\,\mathrm{J/m^2}$, $Ku = 7 \times 10^5\,\mathrm{J/m^3}$, and $\alpha = 0.05 - 0.5$. Stiffness constant $c_{11} = 283 \times 10^9\,\mathrm{J/m^3}$, $c_{12} = 166 \times 10^9\,\mathrm{J/m^3}$, $c_{44} = 58 \times 10^9\,\mathrm{J/m^3}$, mass density $\rho = 8000\,\mathrm{kg/m^3}$, phenomenological elastic damping constant $\eta = 0$ for non-absorbing boundary regions, and the magnetoelastic coupling constants $B_1 = B_2 = 8.8 \times 10^6\,\mathrm{J/m^3}$.[46,47] Due to the limitation of the simulation mesh, the wave speed of 2114 m/s is chosen to obtain at least one full period waveform presented on the strip at low frequencies for a PZT piezoelectric substrate.[37,48]

Since the aim of this work is to achieve acoustic wave-driven motion of skyrmion bags, the injection process is simplified by presetting the magnetization and directly pinning the skyrmion bags onto the ferromagnetic film. First, the radius of the outer circle of skyrmion bag is set to 90 nm, and the inner circles representing skyrmions in the bag distribute equally with a radius of 9 nm. Geometric difference operations are performed between the outer and inner circles to obtain irregular geometric shapes. The area enclosed by this geometry is set

with magnetization $m_z = 1$, and the rest is set to -1. After relaxation, we can obtain regularly and stably distributed skyrmion bags in which inner skymion number N changes from 2 to 9 as shown in Fig. 1(b), located 150 nm to the left of the center of the magnetic nanostrip. As shown in Fig. 1(a), the SAWs were excited at the left of the nanostrip by interdigital transducer (IDT). The displacement is expressed as[36]

$$u_{SH} = \begin{bmatrix} u_x \\ u_y \\ u_z \end{bmatrix} = \begin{bmatrix} 0 \\ A\sin(kx - \omega t) \\ 0 \end{bmatrix}, \quad (4)$$

where u is the displacement, A is the amplitude, k is the wave number, and ω is the frequency of the SAW. Here, high-overtone modes can be used for high-frequency acoustic excitation, and for consistency, the IDT simulation setup mode was used. The shear horizontal (SH) waves (with only shear horizontal displacements) were applied to the nanostrip through the piezoelectric substrate. As an exploration of an additional acoustic excitation method, the response of skyrmion bags driven by circular acoustic waves is presented in Note S1.

To explore the dynamic properties of skyrmion bags driven by surface acoustic waves, the impact of Hall effect induced by high topological charge is vital. The motion of skyrmion bags in the wide ferromagnetic film has been investigated in Fig. S1. Instead, in the narrow strip with a width of 120 nm, the deflection of skyrmion bags is restrained on account of the boundary potential driven by the surface acoustic wave ($f = 10$ GHz, $A = 1$ nm). Figures 2(a)–2(d) show snapshots of the magnetization distribution of the skyrmion bags with N = 3, 5, 7, and 9, respectively. The skyrmion bags are first placed stably at 150 nm from the left of the nanostrip center. When the surface acoustic waves were applied, the skyrmion bags moved along the x-axis without deflection and finally stabilized at the right side of the strip due to high damping. The three moments designated with T0, T1, and T2 refer to 0, 35, and 70 ns, respectively, in Figs. 3(a)–3(d), where the white dashed line denotes the trajectory of the center of skyrmion bags (the positional coordinates of the center obtained by fitting the region with $m_z = 1$). By comparison, it can be seen that the motion distance of skyrmion bags is closely connected with the skyrmion number N at the moment of T2. The average velocities as a function of skyrmion number N are plotted in Fig. 2(e). As can be seen, the average velocity rises sharply when N changes from 1 to 3, following a slow increase, then a decrease for $N > 3$. It ultimately remains constant when N exceeds 8. For $N < 3$, the reaction force generated by the boundary potential pays an increasing acceleration effect on the skyrmion bag as a result of its enlarged size.[49] However, this effect becomes negligible when the size increases beyond this threshold.[24] When $N > 6$, the weak decrease in average velocity results from damping effects due to expansion of the lateral size of the skyrmion bags.

To obtain a faster velocity of skyrmion bags, we investigate how its motion depends on the amplitude, frequency of SAWs, and the material damping, respectively. For comparison, the skyrmion number N is uniformly set to 4 and the nanostrip width is 150 nm. When the frequency and damping remain unchanged ($f = 10$ GHz, $\alpha = 0.1$), the displacement of skyrmion bag is plotted in Fig. 3(a) as the surface acoustic wave's amplitude varies from 0.5 to 1.5 nm. The results in Fig. 3(a) show that the excitation intensity is greater with the amplitude of the SAWs, making the displacement curves steeper, namely faster velocity of the skyrmion bag. Figure 3(b) shows the effect of increasing frequency from 5 to 15 GHz on the motion of skyrmion bag with $A = 1$ nm and $\alpha = 0.1$. The SAWs' shear strain distributions corresponding to different frequencies are shown in Fig. 3(d). For higher frequency acoustic waves, the wavelength is shorter, the strain gradient is sharper, making the skyrmion bags move faster. Furthermore, as shown in Fig. 3(c), the reduction of material damping, from 0.5 to 0.05, remarkably accelerates the skyrmion bag driven by the surface acoustic wave with $f = 10$ GHz, $A = 1$ nm. In contrast, the skyrmion cannot reach a stable magnetization state under excessively low material damping.

Accordingly, we can obtain faster velocity of skyrmion bag by improving the amplitude and frequency of the SAW or decreasing material damping. Nevertheless, the strong driving force causes abrupt shape changes in the inner skyrmion structure, as illustrated by the purple curve corresponding to the magnetization distribution in

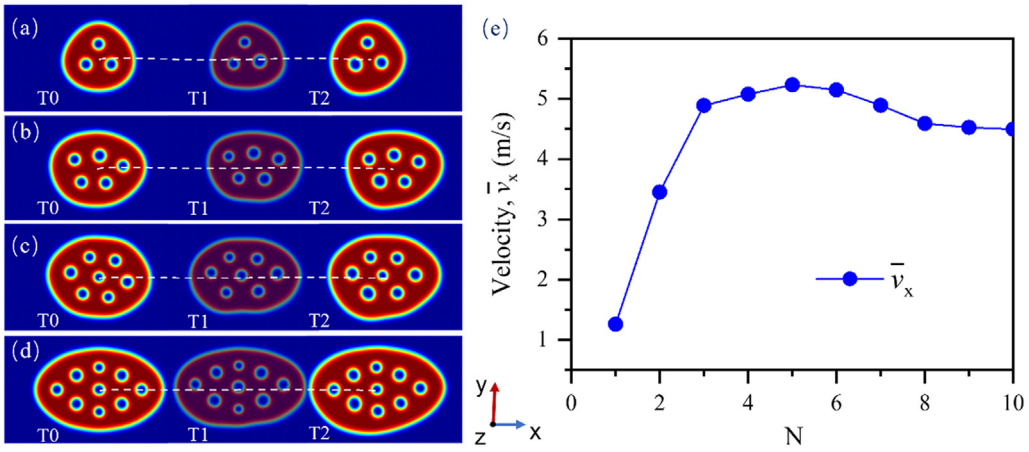

FIG. 2. Skyrmion bags driven by SAWs in the narrow strip. (a)–(d) Snapshots of the magnetization distribution of skyrmion bags with N of 3, 5, 7, and 9, respectively. (e) Average velocity of skyrmion bags vs number of skyrmions N.

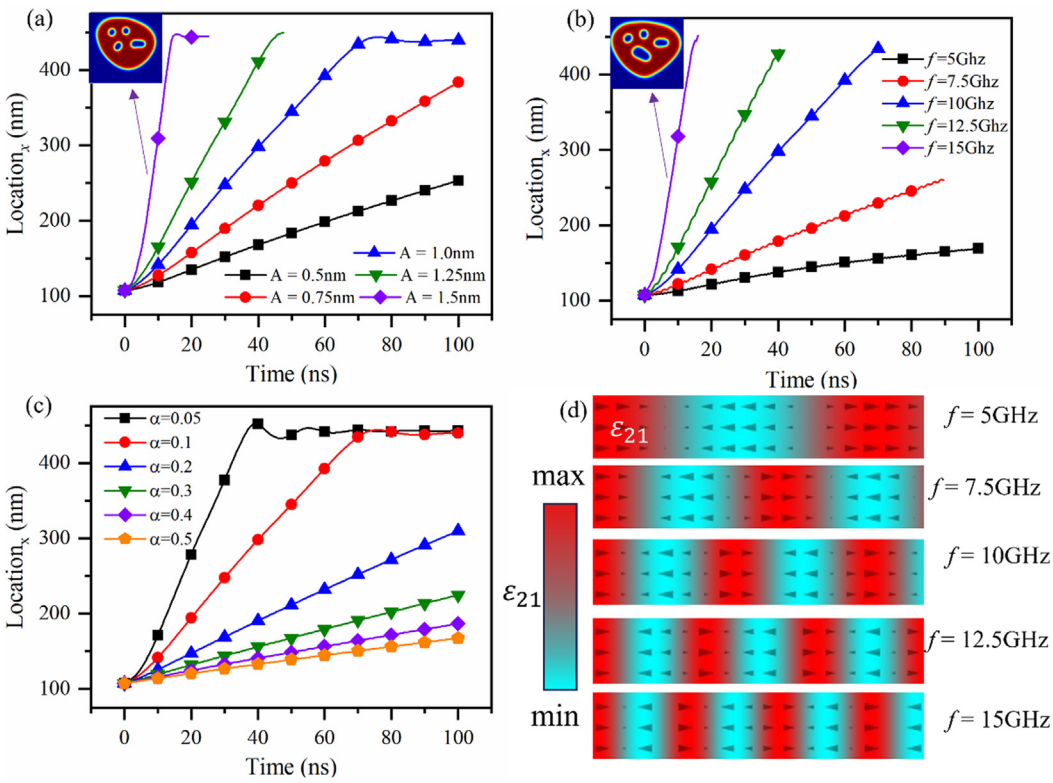

FIG. 3. The displacements of skyrmion bags vs the motion time under varied (a) amplitudes, (b) frequencies of surface acoustic waves and (c) material damping. (d) Distributions of shear strain ε_{21} of surface acoustic waves at different frequencies.

Figs. 4(a) and 4(b). As a result of the alternating driving force induced by surface acoustic waves, the shape of the skyrmion bag is distorted.[50] Excessively high driving force will disturb the magnetization distribution and destroy the morphology of the skyrmion bags, leading to information loss or mismatch. Therefore, it is necessary to choose appropriate SAWs and material damping. Figure S3 displays phase diagrams of dynamical behavior and velocity versus SAW excitation strength, guiding parameter optimization for both driving efficiency and skyrmion bag stability.

A phenomenon of skyrmion bags with rich spin texture has been observed, where the abrupt shape change of inner skyrmions contributes to the acceleration of skyrmion bag. The inner skyrmion undergoes a recoverable deformation where it transforms from regular circular to elliptical shape. Skyrmion deformation results in distance-dependent interaction forces of varying complexity. For the skyrmion bag possessing highly rich spin texture, an abrupt shape change of inner skyrmions tends to form under the strong driving force induced by the surface acoustic wave (see supplementary material Fig. S2). The phase diagram of the abrupt shape change for different N and strip widths in Fig. S2 indicates that skyrmion bags with elevated topological states and reduced boundary confinement potential exhibit a greater propensity for abrupt shape changes.

To explore the origin of shape change, we investigate the magnetization distribution of skyrmion bags with N = 8 and corresponding energy variation under the driving of surface acoustic wave with $f = 10$ GHz and $A = 1.0$ nm in the ferromagnetic strip with width of 300 nm. The movement of skyrmion bags in this case is representative and contains both the progress from steady state to abrupt shape change and the acceleration of skyrmion bag close to the boundary. The velocity of skyrmion bags is displayed in Fig. 4(e), where four regions marked by I–IV indicate different motion states before and after abrupt shape change (see Movie 1 of the supplementary material), from which four typical moments T_1–T_4 are selected, and the corresponding magnetization snapshots are shown in Figs. 4(a)–4(d). The velocity curve in Fig. 4(e) goes exhibits three stages: stage 1, showing steep increase in the velocity v_1 to v_2 caused by mutation in the shape of the skyrmion; stage 2, showing a gradual increase in value from v_2 to v_3 caused by the skyrmion bag contacting boundary; and stage 3, where the velocity stabilizes at v_3 due to the repulsive force of the boundary to the skyrmion bags equilibrating with the Magnus force of the skyrmion bags near the boundary. Notably, from region I to region II, an average velocity increase of approximately 38% reflects the effect of abrupt shape change on the velocity of skyrmion bag.

Further, the time step decreases to 0.025 ns, which equals 1/4 of a wavelength period of surface acoustic wave, more information about the abrupt shape change can be seen at $T_1 = 15$ ns of region II. As illustrated in Fig. 5, the inner skyrmion exhibits not only abrupt shape deformation but also situ rotation and breathing modes. Interestingly, the period of *in situ* rotation coincides with that of surface acoustic wave, while the breathing period equals the half-wavelength, derived

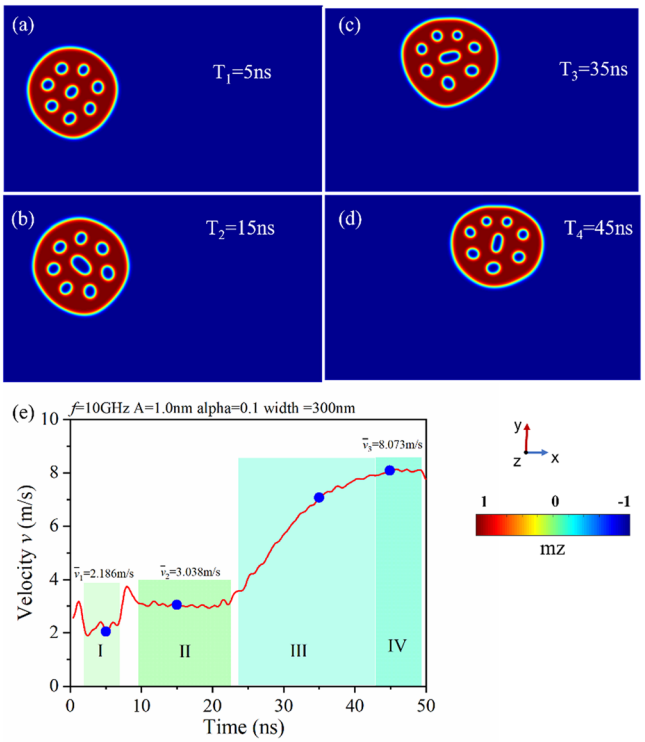

FIG. 4. The instantaneous snapshots of magnetization distribution of skyrmion bags at (a) 5, (b) 15, (c) 35, and (d) 45 ns, respectively (f = 10 GHz, A = 1 nm). (e) Time-varying diagram of average velocity of skyrmion bags driven by SAWs. The blue points correspond to the instantaneous snapshots in (a)–(d).

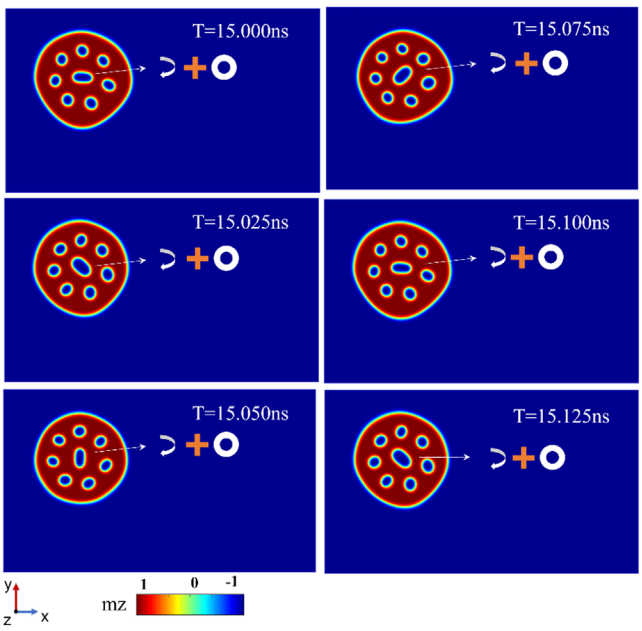

FIG. 5. The instantaneous snapshots of magnetization distribution of skyrmion bags at T = 15.000, 15.025, 15.050, 15.075, 15.100, and 15.125 ns, respectively (f = 10 GHz, A = 1 nm). The white arrow denotes *in situ* rotation and the white circular ring denotes breathing.

from the tensile and compression effect induced by the periodic surface acoustic wave. Besides, the energy variation results in Figs. S4 and S5 manifest that the periodic magnetoelastic coupling energy caused by the surface acoustic wave affects the exchange energy, which leads to the *in situ* rotation and breathing mode of the skyrmion. Due to the small variation in anisotropic energy, the exchange energy dominates the periodic change of total energy (see Movies 2–5 of the supplementary material).

In summary, skyrmion bags driven by surface acoustic waves have been investigated through micromagnetic simulation by numerically solving the Landau–Lifshitz–Gilbert equation and elastodynamics equation. It has been found that the Hall angle and the average speed of movement of skyrmion bags are closely related to the number of inner skyrmions N in the wide ferromagnetic film. Meanwhile, the boundary potential of the narrow strip compels the stretchable skyrmion bags to move without deflection. Moreover, the velocity of skyrmion bags can be effectively manipulated by the magnetic damping constant as well as frequency and amplitude of the surface acoustic wave. By increasing the amplitude and frequency of the surface acoustic wave and decreasing the material damping constant, the velocity of the skyrmion bag can be significantly increased. For the skyrmion bag possessing highly rich spin texture, an abrupt shape change of inner skyrmions comes into being and accelerates the skyrmion bag, which results from a mode of *in situ* rotation and breath of skyrmion induced by periodic surface acoustic waves. This work suggests that the surface acoustic wave can be utilized to drive the motion of topologically nontrivial skyrmion bags in ferromagnetic thin films, which may hold promise for applications in magnetic devices.

See the supplementary material for additional simulation results, as well as animated visualizations of the magnetization and energy evolution processes.

This work is financially supported by the National Program on Key Basic Research Project (Grant No. 2022YFB3807601) and the National Natural Science Foundation of China (Grant Nos. 12272338, 12432007, 12192214, and 12302207).

AUTHOR DECLARATIONS

Conflict of Interest

The authors have no conflicts to disclose.

Author Contributions

Shengbin Shi: Conceptualization (equal); Investigation (equal); Methodology (equal); Software (equal); Validation (equal); Visualization (equal); Writing – original draft (equal). **Yunhong Zhao:** Methodology (equal); Software (equal); Writing – review & editing (equal). **Peng Han:** Methodology (equal); Software (equal); Visualization (equal). **Jiajun Sun:** Methodology (equal); Resources (equal); Software (equal); Validation (equal). **Rui Zhu:** Writing – review & editing (equal). **Jie Wang:** Project administration (equal); Resources (equal); Supervision (equal); Writing – review & editing (equal).

DATA AVAILABILITY

The data that support the findings of this study are available from the corresponding author upon reasonable request.

REFERENCES

[1]S. Mühlbauer, B. Binz, F. Jonietz, C. Pfleiderer, A. Rosch, A. Neubauer, R. Georgii, and P. Böni, Science **323**(5916), 915 (2009).
[2]T. Adams, A. Chacon, M. Wagner, A. Bauer, G. Brandl, B. Pedersen, H. Berger, P. Lemmens, and C. Pfleiderer, Phys. Rev. Lett. **108**(23), 237204 (2012).
[3]E. Ruff, S. Widmann, P. Lunkenheimer, V. Tsurkan, S. Bordács, I. Kézsmárki, and A. Loidl, Sci. Adv. **1**(10), e1500916 (2015).
[4]H. Du, R. Che, L. Kong, X. Zhao, C. Jin, C. Wang, J. Yang, W. Ning, R. Li, C. Jin, X. Chen, J. Zang, Y. Zhang, and M. Tian, Nat. Commun. **6**, 8504 (2015).
[5]N. S. Gusev, A. V. Sadovnikov, S. A. Nikitov, M. V. Sapozhnikov, and O. G. Udalov, Phys. Rev. Lett. **124**(15), 157202 (2020).
[6]A. Casiraghi, H. Corte-León, M. Vafaee, F. Garcia-Sanchez, G. Durin, M. Pasquale, G. Jakob, M. Kläui, and O. Kazakova, Commun. Phys. **2**(1), 145 (2019).
[7]K. Y. Meng, A. S. Ahmed, M. Bacani, A. O. Mandru, X. Zhao, N. Bagues, B. D. Esser, J. Flores, D. W. McComb, H. J. Hug, and F. Yang, Nano Lett. **19**(5), 3169 (2019).
[8]X. Zhao, C. Jin, C. Wang, H. Du, J. Zang, M. Tian, R. Che, and Y. Zhang, Proc. Natl. Acad. Sci. U. S. A. **113**(18), 4918 (2016).
[9]W. Kang, Y. Huang, C. Zheng, W. Lv, N. Lei, Y. Zhang, X. Zhang, Y. Zhou, and W. Zhao, Sci. Rep. **6**, 23164 (2016).
[10]X. Liang, L. Zhao, L. Qiu, S. Li, L.-H. Ding, Y.-H. Feng, X.-C. Zhang, Y. Zhou, and G.-P. Zhao, Acta Phys. Sin. **67**(13), 137510 (2018).
[11]P. Lai, G. Zhao, H. Tang, N. Ran, S. Wu, J. Xia, X. Zhang, and Y. Zhou, Sci. Rep. **7**(1), 45330 (2017).
[12]G. Chen, Nat. Phys. **13**(2), 112 (2017).
[13]X. Zhang, G. P. Zhao, H. Fangohr, J. P. Liu, W. X. Xia, J. Xia, and F. J. Morvan, Sci. Rep. **5**, 7643 (2015).
[14]Z. Zeng, C. Zhang, C. Jin, J. Wang, C. Song, Y. Ma, Q. Liu, and J. Wang, Appl. Phys. Lett. **117**(17), 172404 (2020).
[15]B. Göbel, I. Mertig, and O. A. Tretiakov, Phys. Rep. **895**, 1 (2021).
[16]D. Foster, C. Kind, P. J. Ackerman, J.-S. B. Tai, M. R. Dennis, and I. I. Smalyukh, Nat. Phys. **15**(7), 655 (2019).
[17]F. N. Rybakov and N. S. Kiselev, Phys. Rev. B **99**(6), 064437 (2019).
[18]C. Kind, S. Friedemann, and D. Read, Appl. Phys. Lett. **116**(2), 022413 (2020).
[19]V. M. Kuchkin, B. Barton-Singer, F. N. Rybakov, S. Blügel, B. J. Schroers, and N. S. Kiselev, Phys. Rev. B **102**(14), 144422 (2020).
[20]J. Tang, Y. Wu, W. Wang, L. Kong, B. Lv, W. Wei, J. Zang, M. Tian, and H. Du, Nat. Nanotechnol. **16**(10), 1086 (2021).
[21]C. Kind and D. Foster, Phys. Rev. B **103**(10), L100413 (2021).
[22]R. Chen and Y. Li, ACS Appl. Mater. Interfaces **14**(26), 30420 (2022).
[23]R. Chen, Y. Li, V. F. Pavlidis, and C. Moutafis, Phys. Rev. Res. **2**(4), 043312 (2020).
[24]Z. Zeng, N. Mehmood, Y. Ma, J. Wang, J. Wang, and Q. Liu, J. Phys.: Condens. Matter **34**(39), 395801 (2022).
[25]Z. Zhang, M. Xu, G. Jiang, J. Zhang, D. Meng, W. Chen, Y. Chen, and C. Hu, J. Appl. Phys. **132**(11), 113901 (2022).
[26]X. Bai, J. Wang, J. Yang, H. Liu, S. Zhang, and Q. Liu, J. Magn. Magn. Mater. **586**, 171231 (2023).
[27]R. Yanes, F. Garcia-Sanchez, R. F. Luis, E. Martinez, V. Raposo, L. Torres, and L. Lopez-Diaz, Appl. Phys. Lett. **115**(13), 132401 (2019).
[28]C. Hu, R. Zhao, L. Ji, W. Chen, S. Bandaru, and X. Zhang, J. Magn. Magn. Mater. **513**, 166954 (2020).
[29]J. Sun, Y. Zhang, and J. Wang, Int. J. Solids Struct. **233**, 111213 (2021).
[30]S. Bandyopadhyay, J. Atulasimha, and A. Barman, Appl. Phys. Rev. **8**(4), 041323 (2021).
[31]M. Foerster, F. Macià, N. Statuto, S. Finizio, A. Hernández-Mínguez, S. Lendínez, P. V. Santos, J. Fontcuberta, J. M. Hernàndez, and M. Kläui, Nat. Commun. **8**(1), 407 (2017).
[32]N. K. Babu, A. Trzaskowska, P. Graczyk, G. Centała, S. Mieszczak, H. Głowiński, M. Zdunek, S. Mielcarek, and J. W. Kłos, Nano Lett. **21**(2), 946 (2021).
[33]J. Puebla, Y. Hwang, S. Maekawa, and Y. Otani, Appl. Phys. Lett. **120**(22), 220502 (2022).
[34]T. Yokouchi, S. Sugimoto, B. Rana, S. Seki, N. Ogawa, S. Kasai, and Y. Otani, Nat. Nanotechnol. **15**(5), 361 (2020).
[35]R. Chen, C. Chen, L. Han, P. Liu, R. Su, W. Zhu, Y. Zhou, F. Pan, and C. Song, Nat. Commun. **14**(1), 4427 (2023).
[36]Y. Yang, L. Zhao, D. Yi, T. Xu, Y. Chai, C. Zhang, D. Jiang, Y. Ji, D. Hou, and W. Jiang, Nat. Commun. **15**(1), 1018 (2024).
[37]R. Nepal, U. Güngördü, and A. A. Kovalev, Appl. Phys. Lett. **112**(11), 112404 (2018).
[38]J. Sun, Y. Zhao, S. Shi, Y. Zhang, and J. Wang, Appl. Phys. Lett. **121**(24), 242406 (2022).
[39]R. Khoshlahni, S. Lepadatu, M. Kouhi, and M. Mohseni, Phys. Rev. B **107**(14), 144421 (2023).
[40]S. Li, K.-X. Li, Z.-H. Liu, Q.-Y. Zhu, C.-B. Zhao, H. Zhang, X.-Q. Shi, J.-L. Wang, R.-N. Wang, and R.-Q. Lian, Chin. Phys. B **32**(11), 117503 (2023).
[41]Z. Zeng, C. Song, J. Wang, and Q. Liu, J. Phys. D **55**(18), 185001 (2022).
[42]A. Vansteenkiste, J. Leliaert, M. Dvornik, M. Helsen, F. Garcia-Sanchez, and B. Van Waeyenberge, AIP Adv. **4**(10), 107133 (2014).
[43]F. Vanderveken, J. Mulkers, J. Leliaert, B. Van Waeyenberge, B. Sorée, O. Zografos, F. Ciubotaru, and C. Adelmann, Open Res. Europe **1**, 35 (2021).
[44]J. Sampaio, V. Cros, S. Rohart, A. Thiaville, and A. Fert, Nat. Nanotechnol. **8**(11), 839 (2013).
[45]P. Metaxas, J. Jamet, A. Mougin, M. Cormier, J. Ferré, V. Baltz, B. Rodmacq, B. Dieny, and R. Stamps, Phys. Rev. Lett. **99**(21), 217208 (2007).
[46]F. Vanderveken, J. Mulkers, J. Leliaert, B. Van Waeyenberge, B. Sorée, O. Zografos, F. Ciubotaru, and C. Adelmann, Phys. Rev. B **103**(5), 054439 (2021).
[47]M. Gueye, F. Zighem, M. Belmeguenai, M. Gabor, C. Tiusan, and D. Faurie, J. Phys. D **49**(14), 145003 (2016).
[48]J. Dean, M. T. Bryan, J. D. Cooper, A. Virbule, J. E. Cunningham, and T. J. Hayward, Appl. Phys. Lett. **107**(14), 142405 (2015).
[49]W. Chen, L. Liu, and Y. Zheng, Phys. Rev. Appl. **14**(6), 064014 (2020).
[50]L. Liu, W. Chen, and Y. Zheng, Phys. Rev. Lett. **128**(25), 257201 (2022).